

Evaluation of Karst Aquifer Water Quality Associated with Agricultural Land Use



Lee Florea

Contents

1	Introduction	158
1.1	Physical Chemistry of Karst Springs	160
1.2	Carbon, its Stable Isotopes, and Land Use	162
1.3	Nitrogen, its Stable Isotopes, and Land Use	163
2	Physical Setting	164
2.1	Hydrogeologic Framework	165
2.2	Redmond Creek Karst Basin	166
2.3	Grayson-Gunnar Karst Basin	168
3	Methods	169
3.1	Field Measurements	170
3.2	Discrete Sampling	170
3.3	Continuous Monitoring	171
3.4	Climate Data	171
4	Results	172
4.1	Field Measurement	172
4.2	Discrete Sampling	172
4.3	Continuous Monitoring	177
5	Discussion	180
5.1	Conduit Function	180
5.2	Chemical Processes	181
6	Synthesis	185
	References	188

Abstract The quality of groundwater in karst aquifers has a direct bearing upon aquatic and human health across significant parts of the ice-free land surface. Data from this study investigate the specific changes to water quality (field chemistry, ion concentrations, carbon and nitrogen isotopes, and trace metals) in the groundwater of karst basins that result from agricultural activities such as concentrated farming. Field measurements, discrete water samples, and continuous monitoring from two karst basins, Redmond Creek and Grayson-Gunnar, in south-central Kentucky

L. Florea (✉)

Indiana Geological and Water Survey, Bloomington, IN, USA

e-mail: lflorea@indiana.edu

provide some insight into the patterns, timing, and source of solute and nutrient flux. Redmond Creek, primarily forested land use and along the plateau margin, has a flashier storm response with lower solute concentrations; allogenic recharge is routed through diamicton. In contrast, Grayson-Gunnar, primarily agricultural land use and a sinkhole plain topography, is less flashy with higher and stable concentrations of solutes; autogenic recharge from the epikarst is modulated by rimstone dams along the flow path. Recharge in Grayson-Gunnar sub-basins arrive at the spring as distinct features in hydrographs and chemographs. A muted epikarst signal arrives more than a day later. Land use impacts water quality in each basin. At Redmond Creek, forests in the recharge area provide organic carbon to recharge. The organic carbon degrades along the flow path, retains its original isotopic signature, and incorporates nitrogen from brines associated with shallow petroleum reservoirs. At Grayson-Gunnar, with residential, agriculture, and livestock runoff, the carbon source varies. Storms produce runoff with carbon degraded from forest litter, nitrogen from synthetic fertilizer and livestock, and phosphate and trace metals from mobilized sediments. Base flow from epikarst storage incorporates labile carbon from corn or animal waste and nitrogen from higher trophic levels.

Keywords Confined animal feeding operation · Cumberland Escarpment · Grayson-Gunnar Cave · Nutrients · Redmond Creek

1 Introduction

Epigenetic karst aquifers have a geochemical signature observable in time series monitoring data that is characterized by a disconnect between the aquifer matrix and the embedded conduit system [1, 2]. This fingerprint is strongly controlled by parameters such as recharge, aquifer storage, and chemical interactions that are derived from the surrounding climate, geology, and overlying land use. Changes to land use have a first-order effect on the chemical composition of groundwater in the critical zone in karst landscapes. When land use in a karst basin transitions from natural conditions to concentrated agriculture, the quality of water emerging from a karst spring may degrade.

This chapter presents data and interpretations on chemical and isotope hydrology and nutrient transport from two karst basins in the Paleozoic carbonates of south-central Kentucky, USA, located along the margin of the Cumberland Escarpment. Neither karst basin represents pristine conditions; however, one basin (Redmond Creek – including an input to the aquifer, Stream Cave (SC), and the output from the aquifer, Sandy Springs (SS)) comprises mixed hardwood and pasture, and the second basin (Grayson-Gunnar – GG) is primarily mixed residential, livestock, and row crops and includes a confined animal feeding operation (CAFO) for poultry (Fig. 1).

It is the CAFO in the GG aquifer that was the original impetus for this study, as CAFOs are an increasingly common practice across karst landscapes of the American Southeast and Midwest. As of 2002, the EPA inventoried about 2,500 animal

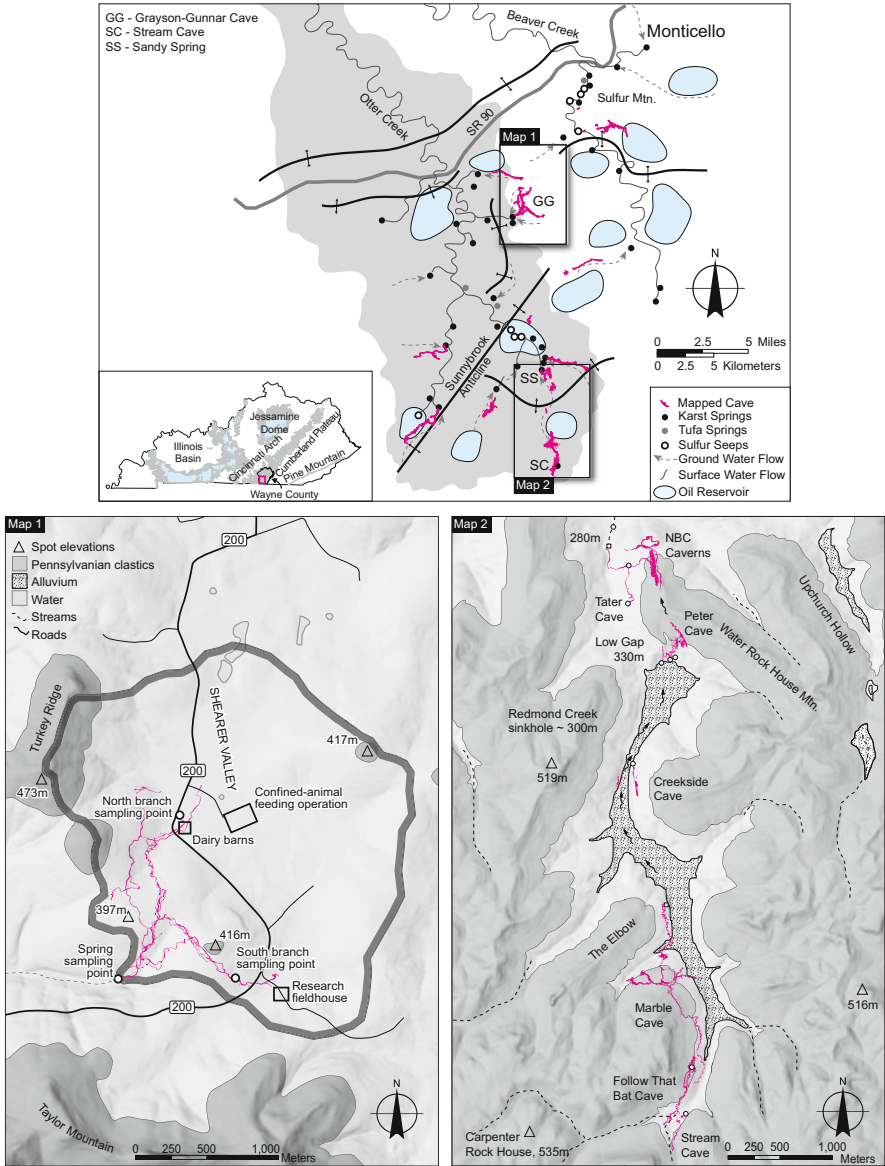


Fig. 1 (Top) The Otter Creek watershed (light gray shaded region) and surroundings in south-central Kentucky USA (inset). Principal karst springs, tufa springs, sulfur seeps, groundwater flow paths, and structural features are shown. Areas of historic petroleum production from shallow reservoirs indicated. Adapted from Figure 1 of Florea [55]. (Map 1) The Grayson-Gunnar karst basin outlined. (Map 2) Redmond Creek karst basin

feeding operations in Kentucky, 10% of which were believed to qualify as a CAFO [3] – defined as having more than 1,000 animal units, equivalent to 100,000 laying hens or broiler chickens [4]. By 2004, 150 of these operations received or planned to

receive permits for discharge management under the National Pollution Discharge Elimination System, NPDES [5]. For 2007 data, Kentucky ranked ninth in the USA for broiler chicken production with an estimated manure production of 1.7 billion kg from all poultry [6]. Specific to Wayne County, the location of this study (Fig. 1), the USDA Census of Agriculture estimated approximately 650,000 broiler chicken in 2012 spread over more than 25 sites. An additional 470,000 laying hens were located in a single facility.

There are significant concerns of the impact that these operations have upon the environment that have resulted in lawsuits and legal settlements, such as between the Sierra Club and Tyson Chicken for two poultry CAFOs in Western Kentucky. In that example, a study by Iowa State University found that these two CAFOs emitted over 900 kg of ammonia in the year they were monitored [7]. While that study was specific to air quality, it illustrates the magnitude of the problem that extends to concerns of water quality, including waste collection and distribution, hormones and antibiotic supplements, and nutritional amendments in feed that include higher concentrations of trace metals, such as copper and selenium.

Limited study has been conducted on the impact of CAFO operations on the quality of water in karst aquifers – the swine facility in Mt. Judea, Arkansas, USA is one notable recent example that has received media attention [8, 9]. Of importance is the potential loading of nutrients from leaking sewage lagoons and spray fields in the case of swine and cattle, and the distributed spreading of the dry waste typical of poultry operations as is found in the northern limits of the GG karst basin (Fig. 1). The Redmond Creek karst basin does not include such operations.

Specific nutrients considered in this study, combined with other chemical and physical parameters from discrete water samples, include dissolved inorganic carbon (DIC) and dissolved organic carbon (DOC), reduced and oxidized nitrogen, and reactive phosphate free in solution and adsorbed onto sediments. Isotopic and other analytical methods are used to better understand the character and source of these nutrients, including how they differ between land use and change as a function of flow condition. Continuous monitoring data of discharge, water chemistry, and nutrient and sediment concentrations in the GG karst basin provide a window into aquifer dynamics during storm events.

1.1 Physical Chemistry of Karst Springs

Karst aquifers in the Paleozoic carbonates of the mid-continent are heterogeneous and anisotropic groundwater systems with highly variable flow regimes and conduit characteristics [10]. These epigenetic karst aquifers are a subsurface extension of surface hydrological systems, with conduit flow linking meteoric recharge at discrete sink points with topographically lower springs [1]. Changes in spring discharge (Q) occur from seasonal or interannual variation in climate or from a single storm event when precipitation exceeds evapotranspiration and the threshold of storage in the soil and epikarst.

Hydrographs and chemographs are the basic tools for understanding the response of a karst spring to hydrologic inputs [11] with the pattern of response guided by three fundamental aquifer attributes: recharge, storage, and transmission [12]. Assuming an instantaneous recharge pulse, the shape of the hydrograph is a manifestation of the transformation of the input signal within the aquifer framework. For example, the delay between the input and hydrograph peak, the lag time, is a measure of the time of travel in the conduit system. Multiple peaks from the same recharge event represent multiple discrete recharge points or conduit bifurcations. The return time to base flow conditions from peak flow after a storm pulse is one measure of the contribution of secondary permeability features, such as bedding planes, fractures, and small conduits. Karst basins dominated by discrete recharge, low storage, and rapid transmission will have short lag times with a ‘flashy’ spring flow hydrograph [1, 10, 13]. This behavior, measured using the Q ratio:

$$Q_{\text{ratio}} = \frac{Q_{\text{max}}}{Q_{\text{mean}}}, \quad (1)$$

where Q is discharge, shows that a high Q_{ratio} (flashy behavior) characterizes most karst springs along the Cumberland Escarpment [14]. In contrast, karst basins with diffuse recharge, high storage, and slow transmission will have long lag times, a diminished spring flow hydrograph, and a lower Q_{ratio} [15]. Included in this second category are large karst basins and karst aquifers in young limestone that retain significant primary porosity and permeability [10].

The chemical character of spring flow is greatly influenced by the timing and mode of recharge, aquifer characteristics, overlying land use, and water-rock interactions along the flow path [17, 18]. Periods of more frequent storm events lead to increased discharge from meteoric recharge delivering surface temperature (T) water and lower dissolved solids and therefore lower specific conductance (SpC) and pH . These same events, however, may convey greater concentrations of dissolved oxygen (DO), suspended solids (turbidity), nutrients, and anthropogenic contaminants, such as certain metals, than present in the aquifer during base flow.

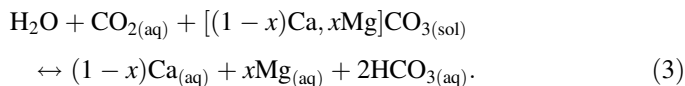
At the scale of individual storm events, chemographs may communicate detailed information about the interaction of recharge with the aquifer framework. Desmarais and Rojstaczer [18] divide storm events in epigenetic karst into three stages based on the SpC chemograph: flushing, dilution, and recovery. The flushing stage, observed by Ryan and Meiman [19] in the Big Spring karst basin of Mammoth Cave National Park, Kentucky, USA, includes a short pulse of higher SpC water forced from aquifer storage just as water levels begin to rise. Multiple negative excursions of SpC and pH (and either positive or negative T excursions) can be an indication of multiple sources of recharge or bifurcating flow paths in the aquifer. The peaks of these excursions may not align with maximum discharge, particularly in aquifers with significant storage or where discharge is driven by piston flow. Recovery time for SpC , pH , T , ion concentrations, and nutrient levels may differ among parameters and vary by season; return to base flow characteristics may be modulated by reaction time of chemical process, draining of secondary permeability, and contributions from epikarst storage.

1.2 Carbon, its Stable Isotopes, and Land Use

Carbon occurs as two stable isotopes, ^{12}C and ^{13}C . The enrichment or depletion of the heavier isotope in a natural system is governed by fractionation processes, such as water-rock interactions, photosynthesis, and metabolic pathways that preferentially select or release one isotope of carbon over the other [20]. Because the abundance of ^{13}C is approximately 1.1%, the ratio of the two can be analytically determined in natural materials and compared to the international Vienna Pee Dee Belemnite (VPDB) reference standard, denoted as $\delta^{13}\text{C}$ and calculated using

$$\delta^{13}\text{C}(\text{‰}) = \frac{^{13}\text{C}/^{12}\text{C}_{\text{sample}} - ^{13}\text{C}/^{12}\text{C}_{\text{VPDB}}}{^{13}\text{C}/^{12}\text{C}_{\text{VPDB}}} \cdot 1000. \quad (2)$$

In shallow groundwater of karst landscapes, values of $\delta^{13}\text{C}$ derive from dissolved organic and inorganic carbon ($\delta^{13}\text{C}_{\text{DOC}}$ and $\delta^{13}\text{C}_{\text{DIC}}$) sourced to the atmosphere, organic matter at the land surface and within the soil column, the isotopic composition of the carbonate bedrock, and the organic carbon in the bedrock. These end members (each with known ranges of $\delta^{13}\text{C}$) are processed in the karst aquifer by microbiologic reactions, limestone dissolution, and gas-water exchange processes controlled by the carbonate equilibrium reaction, broadly written as



The variables x and $1-x$ are proportional to the fraction of dolomite and calcite reacting with the groundwater, respectively.

Values of $\delta^{13}\text{C}_{\text{DOC}}$ have a predictable association with biological process. For example, photosynthesis preferentially utilizes ^{12}C during carbon fixation [21, 22]. The resulting $\delta^{13}\text{C}_{\text{DOC}}$ of vegetation depends upon plant type: native plants in humid landscapes (mixed hardwood and flowering plants) primarily use the C3 pathway, which yields organic matter with $\delta^{13}\text{C}$ values between -23‰ and -27‰ . Plants more adapted to arid conditions commonly use the C4 pathway that yields $\delta^{13}\text{C}$ values between -10‰ and -14‰ . Dissolved organic matter (DOM) in groundwater as humic, fulvic, or other organic acids, including animal waste, degrades into secondary byproducts. These less labile organic molecules absorb more ultraviolet (UV) radiation. At a wavelength of 365 nm, DOM fluoresces visible light with a peak wavelength of 480 nm. Measurements of this fluorescence, fDOM, can provide one measurement of the concentration of organic matter in water. At a wavelength of 254 nm, peak UV absorption occurs, and when normalized to the concentration of DOC, this specific UV absorption (SUVA) value provides one measure of nutrient source (how labile the carbon is) that can supplement measurements of $\delta^{13}\text{C}_{\text{DOC}}$ [23].

Equation 3 shows that the carbon flux through karst groundwater combines bedrock sources with atmospheric and biologic processes that generate CO_2 in solution. In a closed system, waters undersaturated with respect to carbonates would theoretically have values of $\delta^{13}\text{C}_{\text{DIC}}$ that more reflect the organic matter that produces soil CO_2 . Saturated solutions would have an ideal $\delta^{13}\text{C}_{\text{DIC}}$ that is a 50% blend of soil and bedrock sources of carbon. Despite known $\delta^{13}\text{C}$ ranges for atmospheric and biologic sources of carbon, the quantified fractionation when dissolving carbon dioxide into water [24], and the predictable association of bedrock carbon with stratigraphy, the interpretation of $\delta^{13}\text{C}_{\text{DIC}}$ in karst groundwater is significantly more complex than a simple mixing of end members. Rather, in open systems, one must consider phases of CO_2 enrichment or degassing along the flow path [25, 26]; alternative water-rock interactions, such as those associated with sulfur and nitrogen, that may release DIC into an aqueous solution without corresponding soil CO_2 ; or by siliciclastic weathering that sequesters CO_2 from the atmosphere without the addition of bedrock DIC [27]. In summary, changes in end-member contributions to DOC and DIC (e.g., vegetative cover and bedrock composition) as well as variations in the hydraulic function of the underlying aquifer system from droughts or storm events may manifest as changes to the values of $\delta^{13}\text{C}_{\text{DIC}}$. Florea [28] investigated these processes in measurements of $\delta^{13}\text{C}_{\text{DOC}}$ and $\delta^{13}\text{C}_{\text{DIC}}$ from the Redmond Creek karst basin and found $\delta^{13}\text{C}_{\text{DOC}}$ values that were relatively stable and the product of C3 vegetation and $\delta^{13}\text{C}_{\text{DIC}}$ values that varied according to discharge and calcite saturation state.

1.3 Nitrogen, its Stable Isotopes, and Land Use

Nitrogen is involved in biogeochemical processes and is a limiting nutrient in ecological function [29]. The nitrogen cycle involves a complex suite of feedbacks involving redox reactions. These reactions govern availability and the availability of nitrogen in soils through atmospheric deposition, and bacterial denitrification is a key aspect of primary productivity. Soil amendments of ammonia enhance primary production; however, exports of excess ammonia and nitrified products (nitrite and nitrate) lead to excess nutrients and eutrophication of surface water. In karst aquifers, excess nitrogen may travel long distances underground without biologic uptake. Therefore, unmanaged collection and distribution of manure from concentrated agriculture and synthetic fertilizers may leach into underlying conduits.

Nitrogen also occurs as two stable isotopes, ^{14}N and ^{15}N , with ^{15}N comprising <0.4% of total nitrogen. The ratio of the two, $\delta^{15}\text{N}$, can be analytically determined in natural materials and compared to atmospheric molecular nitrogen as a reference standard, calculated using

$$\delta^{15}\text{N}(\text{‰}) = \frac{\frac{^{15}\text{N}}{^{14}\text{N}}_{\text{sample}} - \frac{^{15}\text{N}}{^{14}\text{N}}_{\text{atm}}}{\frac{^{15}\text{N}}{^{14}\text{N}}_{\text{atm}}} \cdot 1000. \quad (4)$$

Synthetic fertilizers, produced from atmospheric sources, typically have $\delta^{15}\text{N}$ values within a narrow range from -2‰ to $+2\text{‰}$ [30]. Because nitrogen fixation in plant materials involves biotic and abiotic processes, such as atmospheric deposition of natural and anthropogenic NO_x (-3‰ to $+1\text{‰}$), geologic sources (-11‰ to $+24\text{‰}$), microbial symbiosis in legumes ($+2.5\text{‰}$ to $+6.3\text{‰}$), and various intra-plant fractionation processes [31], $\delta^{15}\text{N}$ values within vegetation, and therefore natural soil organic matter, have a much wider global range ($>35\text{‰}$) [32]. These data, however, largely concentrate from 0‰ to $+6\text{‰}$. For example, Holá et al. [33] found a $\delta^{15}\text{N}$ value of $+4.2\text{‰}$ for a controlled source of feed corn. Metabolic processes produce animal waste enriched in ^{15}N compared to diet because of NH_3 volatilization, such that values of $\delta^{15}\text{N}$ will increase by $2\text{--}3\text{‰}$ with each trophic level. For example, Inácio et al. [34] measured $\delta^{15}\text{N}$ values of $+14.9\text{‰}$ in poultry manure. Conversely, the ratio of total organic carbon to total nitrogen (C:N ratio) decreases with lower diet qualities at higher trophic levels; ideal C:N ratios in soil are 24:1 [35].

Thus, in groundwater, combined values of $\delta^{15}\text{N}$ and C:N ratios may be one method to broadly discriminate between nitrogen sources associated with synthetic fertilizers, plant material, and animal waste. Runoff from unaltered land uses should have ideal $\delta^{15}\text{N}$ and C:N values centered on $+3\text{‰}$ and 24:1, respectively. In contrast, runoff from row crop land uses would produce recharge with $\delta^{15}\text{N}$ and C:N values centered on 0‰ and 10:1, assuming synthetic fertilizers were the primary nitrogen source. Contributions of septic systems and animal manure would enrich recharge in ^{15}N and further deplete C:N ratios. The association between land use and the concentration and isotopic profile of DOC and total nitrogen are presented in detail by Cravotta [36] for a multi-year investigation in the Susquehanna River watershed of Pennsylvania.

2 Physical Setting

The US Interior Plateaus are a portion of Ecoregion IX as defined by the US Environmental Protection Agency [37]. They span some 128,000 km² west of the Appalachian Mountains from southern Ohio to northern Alabama and include major portions of both Kentucky and Tennessee, including most of the watershed of the Cumberland River. Key characteristics of this region include rolling hills and valleys ranging from 100 to 600 m above mean sea level (amsl), irregular plains and tablelands (e.g., Highland Rim, Pennyroyal Plateau) bounded by escarpments (e.g., Dripping Springs, Muldraugh's Hill, and Cumberland) along significant geologic boundaries on the margin of structural domes of the Cincinnati Arch (Jessamine and Nashville), and deeply incised rivers (e.g., Cumberland, Green,

Kentucky, and Licking) with a geomorphology that is the product of repeated cycles of incision/aggradation during post-Miocene glaciation [38, 39]. To the east are the more mountainous Cumberland Plateau and Appalachian Basin and to the west are the lower elevation plains of the Illinois Basin and Mississippi Embayment.

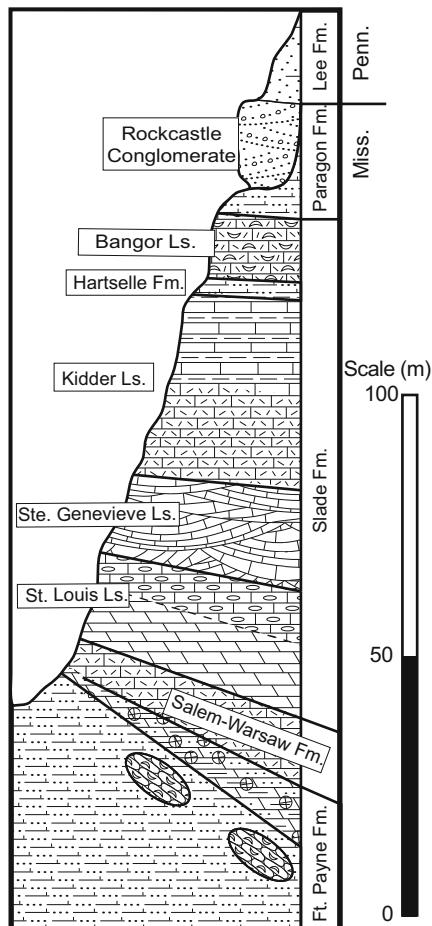
The geology of Interior Plateaus comprises near-horizontal layers of Ordovician through Middle Carboniferous carbonates and siliciclastics. Devonian and Early Carboniferous siltstone and shale erode easily and evolved into retreating escarpments. These escarpments are heavily forested with humid-temperate hardwood, and separating broad exposures of carbonates that karst processes have slowly denuded. The results are extensive sinkhole plains underlain by dense fragipan soils [40]. The sinkhole plains are a mature karst landscape underdrained by integrated conduit systems conveying recharge from the average 120 cm of annual precipitation to springs along base-level streams and rivers. The sinkhole plains and other plateau surfaces supported expansive oak-dominated forests and savannah-like grasslands prior to settlement; now they are largely open pastureland (cattle and horse) and row crops (soybean, corn, and tobacco).

The Interior Plateaus experienced steady population growth between 1970 and 2000 – increasing 40% from 4.4 to 6.2 million. Urbanization in large metropolitan centers of Nashville, Tennessee (1.87 million, an increase of 30% since 2000) and Lexington, Kentucky (0.72 million, which increased 16% between 2000 and 2010) have been a major factor in this growth. The change in land use between 1973 and 2000 was 4.3% [41], largely from the expansion of developed land and through conversion of forests to agriculture. In 2004, 12% of forest landowners surveyed in Kentucky planned to sell their lands, pass it on to heirs, or convert it to another land use including subdivisions [42]; the US Forest Service ranked south-central Kentucky 6th and 12th in the USA for forest fragmentation and loss, respectively [43].

2.1 Hydrogeologic Framework

Along the Cumberland Escarpment of south-central Kentucky (Fig. 1), rugged terrain with more than 230 m of local relief results from the differential erosion between a resistant “caprock” of Middle Carboniferous sandstones and conglomerates and the underlying carbonate system, including the relatively pure limestone and dolomite of the Slade Formation and the calcareous shale of the Paragon Formation [44] (Fig. 2). Tiered levels of relict conduits, preserved along the escarpment margin, track staged incision of base level during interglacial phases in the Plio-Pleistocene [45–48]. Active cave streams descend steeply through the stratigraphy, impeded by less soluble horizons [49], with tributaries collecting into sinuous main stem conduits near the water table [50, 51] that emerge as gravity-flow springs at the base of the escarpment or the contact with the underlying, less soluble strata [49].

Fig. 2 Stratigraphic column illustrating the stratigraphy of the Cumberland Escarpment along the eastern margin of the US Interior Plateaus in south-central Kentucky. Reprinted, with permission, from Figure 2 of Florea [55]



2.2 Redmond Creek Karst Basin

Sandy Springs is the headwaters of Otter Creek, a third-order tributary of the Cumberland River (Fig. 1). Dye tracing has verified that the water in Sandy Springs emerges from the Redmond Creek karst basin with headwaters located 7.5 km south in Tennessee [52]. The carbonate outcrop occupies about 23% of this 1,906-ha watershed, with the remaining landscape underlain by siliciclastics atop the Cumberland Plateau. The central feature of the watershed is a single alluviated sinkhole that measures approximately 4-km long by 1-km wide, which occupies most of the carbonate exposure and captures virtually all allogenic runoff from the plateau via sinking streams, such as Stream Cave near the headwaters of the watershed. Surrounding this sinkhole, more than 16-km of cave passages have been surveyed at six principal elevations among 45+ known caves which span the

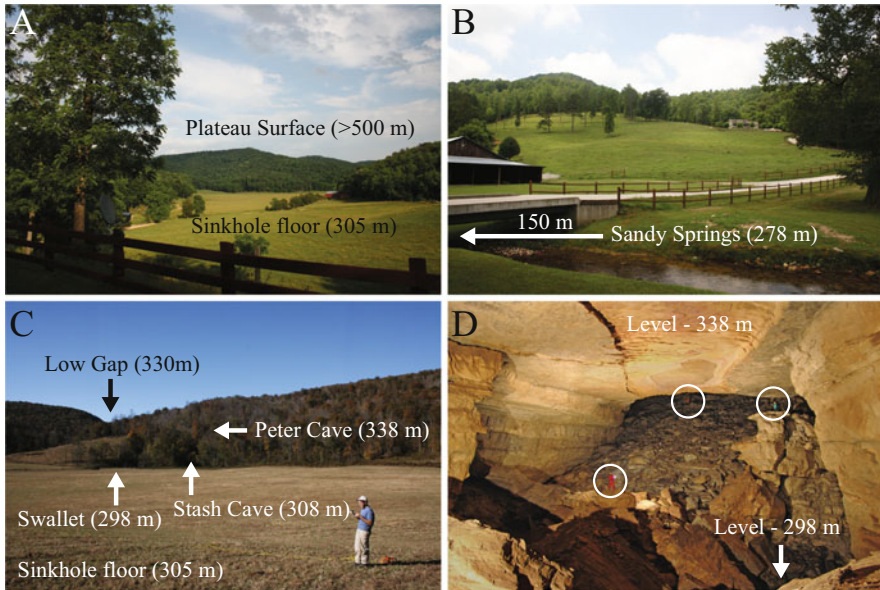


Fig. 3 Photos from the Redmond Creek study area (a) Typical landscape with uplands of the Cumberland Plateau underlain by clastics and the alluviated sinkhole floor. (b) The sampling and monitoring point for water chemistry located at the headwaters of Otter Creek near SS. (c) Elevation relationship among caves and landforms at the downstream end of the Redmond Creek sinkhole. (d) The large chamber in the cave that feeds SS. Individual caves are circled. All photos are by the author except for d, which is courtesy of Sean Roberts. Source: Author

thickness of the carbonate sequence [48]. Near Sandy Springs, cave levels coalesce via collapse and passage cross sections can exceed 3,500 m² (Fig. 3).

The Redmond Creek karst basin is minimally impacted by human activities, being primarily woodland with a history of selected timber harvesting dating back to the early 1900s (Kay Koger, landowner – personal communication). Open pasture and light agriculture occupy the sinkhole floor and the estimated population density is ~0.01 ha⁻¹ with all households on residential septic. Redmond Creek carries water only during high flow and meanders some 6.6 km between Stream Cave and the northern terminus of the sinkhole, the normally dry streambed traverses atop thick alluvium that blankets the sinkhole floor to a depth of >20 m [53]. Along the sinkhole margin, ‘phreatic lifts’ in several caves convey pressurized floodwaters from passages often concealed by cobbles, organic debris, or water. Thus, aquifer water likely drains through a combination of conduits and alluvium [14] prior to rising from a sump and flowing 1 km through a large cave before emerging at Sandy Springs.

Recharge to the Redmond Creek karst basin, and by extension other karst basins in the region, has a seasonal bias toward winter months and only occurs when a threshold of precipitation has been achieved that exceeds PET, observable in the stable isotopes of water [16]. Shallow brines associated with petroleum reservoirs in

Early Carboniferous strata also have an impact upon the chemistry of spring water at Sandy Springs; sulfate and chloride concentrations covary independent of nutrients or ions associated with carbonate dissolution [54, 55]. From the stoichiometry of carbonate equilibrium reactions (Eq. 3) compared with results of discrete samples from Sandy Springs, Florea [48], comparing calcium and magnesium concentrations to the concentration of bicarbonate, estimated the potential for carbonate dissolution from the oxidation of reduced sulfur was upwards of 29%. The prevalence of petroleum seeps enriched in sulfur across the Otter Creek watershed suggests that this is not a localized phenomenon [55]. Using a mass balance approach and continuous monitoring data from Sandy Springs, Florea [48] provided estimated landscape denudation rates of 13.1–17.9 mm/ka, significantly lower than the 48.5 mm/ka found by Paylor [56] in the Blowing Cave karst basin, 5 km to the west. In that study, particulate inorganic carbon (PIC) contributed up to 10% of the total carbon load in an aquifer that was largely not alluviated.

2.3 Grayson-Gunnar Karst Basin

The Grayson-Gunnar karst basin includes one of two springs that comprise Double Head Springs, a first-order tributary of Otter Creek and 8 km north of Sandy Springs (Fig. 1). The Grayson-Gunnar spring is the only known entrance to an 11-km-long cave system divided into two levels: an upper relict level in the lower Ste. Genevieve limestone and a lower canyon that includes two underground streams comprising much of this cave system and descending along the flow path through the thickness of the St. Louis limestone (Fig. 4).

The underground streams drain a karst basin with an estimated size of 496 ha, and groundwater divides, not yet defined by dye tracing, separate the Grayson-Gunnar karst basin from others to the north. The approximate northern limit of the basin are



Fig. 4 Photos from the Grayson-Gunnar study area. (a) Landscape in Shearer Valley bordered by remnants of the Cumberland Escarpment that illustrates intense row-crop agriculture (soybean in this photo from 2017, corn in 2015), livestock barns, and the top of the poultry CAFO facility. Photo is looking north. (b) Ponds perched on the insoluble Lost River Chert at the north end of the karst basin in Shearer Valley. Photo is looking east. (c) Main underground stream in Grayson-Gunnar Cave with visible rimstone dams. Photos a and b are by the author, c is courtesy of Robert Coomer

two ponds perched on chert, which have changed shape and size many times between 1990 and the present day (Fig. 4). The Grayson-Gunnar karst basin is further from the escarpment and up the stratigraphic dip; thus, carbonate exposures characterize more than 80% of the landscape, largely in Shearer Valley. This valley is a broad, flat-floored sinkhole plain perched at the elevation of the Lost River Chert, a regionally pervasive zone of bedded chert centered 4.6 m above the contact between the St. Louis and Ste. Genevieve limestones [57] (Fig. 2).

Population density in the Grayson-Gunnar karst basin is more than five times that of Redmond Creek. The stream in the south branch of the Grayson-Gunnar karst basin, the H-Passage in the survey data (Fig. 1), rises from small pools and for more than a kilometer cascades through a series of travertine waterfalls spaced tens of meters apart and each ranging from 0.3 to 1-m tall. The land use overlying the recharge area to the H-Passage includes low-density grazing and residential septic tanks (including the field house from which this study was conducted).

The land use overlying the stream in north branch of the Grayson-Gunnar basin, the P-Passage in the survey data (Fig. 1), includes significant row crops (corn at the time of this study), a small-scale dairy farm, and a poultry CAFO with six, 150-m-long barns constructed between 1997 and 2003 (Fig. 4). The mapped underground stream is less than 25 m beneath the dairy barns and extends to within 200 m of the CAFO. At the upstream passage terminus, water rises from a sump and flows in a deepening canyon for approximately 1 km to where the north and south branches converge in an anastomotic catacomb of partly water filled tubes. For 600 m from the confluence to the spring, the G passage in the survey data, the combined water cascades over rimstone dams and travertine waterfalls ranging from 0.5 to 1.5-m-tall and spaced an average of 50 m apart (Fig. 4). All rimstone dams and travertine in the underground streams are coated with a thin film of clay and appear to not be actively forming.

3 Methods

Data considered in this study comprise two time periods and frequencies for field chemistry and discrete samples: 16 sets of bimonthly samples from Sandy Springs and Stream Cave at Redmond Creek (Fig. 1) with concurrent monitoring data that span from July 2010 to February 2011; and 10 weekly discrete samples from Grayson-Gunnar from May to August of 2015 (including four sets of samples from the H- and P-Passage; Fig. 1) with supplemental field measurements, samples, and monitoring data that extend from March to December of 2015. Sample collection and analytical methods for the study at Grayson-Gunnar are presented herein and are more comprehensive than the study at Redmond Creek. Data collection for Sandy Springs and Stream Cave include somewhat different but analogous equipment models and analytical methods extensively described in earlier publications [16, 28, 48].

Despite the separation of several years, both datasets come from periods with similar precipitation totals that are greater than the average of the 4 years before each period of study (data from the Kentucky Mesonet, <http://kymesonet.org/> accessed

September 6, 2017, for a nearby station in Albany, KY, Latitude: 36.71°N Longitude: -85.14°). The data from each aquifer also include seasonal transitions and significant storm events separated by extended periods of limited precipitation. Therefore, these data reveal hydrologic and chemical patterns typical of each aquifer, which are similar in scale. This allows for direct comparison based upon differences in hydrogeological framework and land use; they provide additional insight into karst landscapes.

3.1 Field Measurements

Field data include measurements of pH, SpC, T, and DO collected using handheld sondes, a YSI ProPlus at Grayson-Gunnar, calibrated prior to each visit. Measurements of instantaneous Q at the Grayson-Gunnar spring were computed using a Type A current meter and standard USGS gauging techniques (e.g., [58]). Onsite alkalinity data were acquired using a HACH digital titrator with 1.6N H_2SO_4 . The inflection point method, using the USGS alkalinity calculator (<https://or.water.usgs.gov/alk/>), was used to determine the concentration of carbonate species to an accuracy of approximately 4% [59]. At Grayson-Gunnar, dual titrations with filtered and unfiltered water provided one measure of DIC and the suspended load fraction of particulate inorganic carbon (PIC), respectively [56].

3.2 Discrete Sampling

Laboratory analyses were conducted on samples filtered through a $0.45\ \mu\text{m}$ syringe filter and kept at 4°C . Samples for nutrient speciation were collected in a 250 mL HDPE bottle and analyzed within 48 h. Speciation of nitrogen (NH_3 , NO_2 , NO_3) and orthophosphate (PO_4) were quantified using a HACH DR 2800 portable spectrophotometer. Samples for ion analysis (SO_4 , Cl, Na, K, Ca) were collected in 250 mL HDPE bottles, the cations preserved using 2 mL of 6N HNO_3 , and analyzed using a Dionex 3000 ion chromatograph at the Ball State University (BSU) Organic Chemistry laboratory. An aliquot of the cation sample was sent to the Bureau of Water Quality in Muncie, Indiana for trace metal analysis (Pb, Cr, Cu, Ni, Se, Sb) using chromatography methods.

Values of Mg were not available from the IC analysis and were estimated using a 44% contribution of dolomite to the chemistry of spring water because it matches the measured foot-by-foot composition of the enclosing St. Louis and Ste. Genevieve limestones as determined by XRD [57]. This contrasts with dolomite contributions of 29% measured in the Redmond Creek aquifer [48] because recharge to and flow through the Grayson-Gunnar aquifer principally occurs at or below the Lost River Chert as compared to the entire thickness of the Mississippian carbonate sequence at Redmond Creek.

Samples for DIC and DOC concentration were collected in 40 mL septum-capped glass vials and analyzed in the BSU Organic Chemistry laboratory using stepped CO₂ purging with HNO₃ for DIC and persulfate digestion for DOC on a Sievers 900 carbon analyzer. Specific ultraviolet absorbance (SUVA) for the DOC in solution was obtained at a 254-nm wavelength using a SUVA analyzer on unreserved samples.

Samples for the isotopic ratio of carbon ($\delta^{13}\text{C}$) in DIC were collected in a 15-mL vial spiked with copper (II) sulfate and sealed with parafilm. The isotopic ratios for the Grayson-Gunnar samples were analyzed at BSU laboratory using a Picarro cavity ring-down spectroscopy (CRDS) system paired with phosphoric acid digestion to produce CO₂ from the DIC in solution. Samples for the stable isotopes of carbon ($\delta^{13}\text{C}$) and nitrogen ($\delta^{15}\text{N}$) in the DOC were collected in 1-L Nalgene bottles preserved with 1 mL of 12N HCl and sealed with parafilm. In the lab, samples were dehydrated and treated with sulfurous acid to remove residual inorganic carbon. The remaining organic resin, loaded in tin capsules, were sent to the stable isotope lab at the University of South Florida for analysis on a Thermo Fisher Delta V isotope ratio mass spectrometer using a Costech combustion module to produce CO_x and NO_x from the capsules. Isotopic results for carbon were compared to the VPDB reference standard; nitrogen results were compared to the atmospheric reference.

3.3 *Continuous Monitoring*

Between site visits, an In-Situ Aqua Troll 200 sonde deployed near the Grayson-Gunnar entrance collected values of water level (WL), SpC and T every 10 min. At the same time interval, a YSI EXO2 sonde measured pH, DO, turbidity, fDOM, and phycocyanin (a water-soluble accessory pigment to chlorophyll). The sondes were calibrated prior to and after deployment, with additional calibrations for the EXO2 during monthly data downloads and battery replacements. Original data downloaded from the sondes were archived in Microsoft Excel with short gaps in data coverage interpolated from bounding data. Regression models were applied to correct for instrument drift between calibrations, when appropriate. Sonde measurements of WL are converted to discharge using a rating curve developed from the field measurements of instantaneous Q .

3.4 *Climate Data*

Two sources of daily precipitation data were used to create an average value for the Grayson-Gunnar aquifer, the KY Mesonet data from Albany, KY and a privately maintained NOAA cooperorator site near Monticello, KY (Station ID – GHCND: US1KYWY0001, <https://www.ncdc.noaa.gov>; accessed February 24, 2017; latitude, 36.82°N; longitude, -85.01°). Additional data from the Mesonet site include

average daily air temperature and solar insolation. Combined with the average precipitation, these data were used to compute the daily potential evapotranspiration using the Priestley-Taylor method [60], given by

$$\text{PET} = 1.26\alpha \frac{[Q_n/\rho\lambda]}{\alpha - 1}, \quad (5)$$

where α is the Penman ratio, Q_n is the solar insolation in $\text{cal}/\text{cm}^2\text{-day}$, ρ is the fluid density, and λ is the fluid viscosity. The average daily temperature is used to compute the Penman ratio, the fluid density, and the fluid viscosity. The potential daily recharge to the aquifer is given as the sum of the average precipitation and the PET minus 50% of the PET for the subsequent day and 25% of the PET for the day after. Recharge is assumed to be 0 if the sum of the precipitation and PET yields a negative result.

4 Results

4.1 Field Measurement

Temperatures for Grayson-Gunnar during the period March 21, 2015–September 5, 2015, range between 13.7°C and 14.5°C with a warming trend through the summer (Fig. 5). SpC values are consistent with regional karst groundwater and increase during the summer from 300 to 400 $\mu\text{S}/\text{cm}$. In contrast, pH values decreased from 8.26 to a minimum of 6.8 during this same period. DO values ranged between 9 and 11 mg/L with no specific trend. Field measurements of DO from the sampling sites in the north and south branch of Grayson-Gunnar generally agree with the values at the spring, except for DO on May 16, 2015, when values in both branches were anomalously lower – approximately 7.65 mg/L . Temperature values from Sandy Springs are in the same range; however, the average values of SpC, pH, and DO are significantly different compared to Grayson-Gunnar – 207 $\mu\text{S}/\text{cm}$, 7.7, and 11.2 mg/L at Sandy Springs compared to 346 $\mu\text{S}/\text{cm}$, 7.3, and 10.4 mg/L at Grayson-Gunnar. While average values of SpC at Stream Cave reveal less interaction with bedrock (41 $\mu\text{S}/\text{cm}$); the average values of pH and DO are similar to the results at Grayson-Gunnar (7.3 and 10.6 mg/L).

4.2 Discrete Sampling

Results of ion chemistry for discrete samples for the period March 21, 2015–September 5, 2015, for Grayson-Gunnar are presented in Fig. 6. Charge balance errors of these samples average 2.1% with all but three samples at or below 11%.

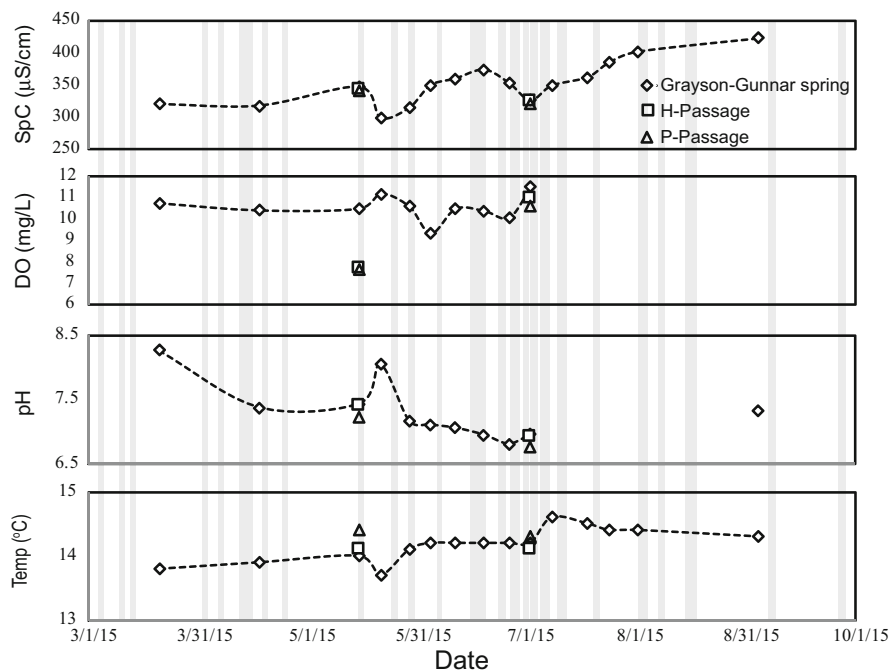


Fig. 5 Graphs of field chemistry from the Grayson-Gunnar karst basin spring through fall of 2015. Measurements collected using a calibrated YSI ProPlus multiparameter sonde. Solid light-gray bars are periods of significant precipitation

The three samples with charge balance errors between 13% and 19% are from July 3, 2015, during a high-flow event. Average Ca, Mg, Na, and K concentrations at the Grayson-Gunnar spring (1.08, 0.24, 0.57, and 0.11 mmol/L) are greater than values at Sandy Springs (0.95, 0.18, 0.16, and 0.02 mmol/L) and at SC (0.13, 0.05, 0.03, and 0.01 mmol/L). Average concentrations of Cl and SO₄ at Grayson-Gunnar (0.12 and 0.08 mmol/L) are comparable but slightly lower than those at Sandy Springs (0.15 and 0.09 mmol/L) but greater than at Stream Cave (0.03 and 0.04 mmol/L). While concentrations of Na and K at Grayson-Gunnar do not reveal any specific trends, concentrations of Cl and SO₄ at Grayson-Gunnar are at their lowest during significant periods of rainfall (Fig. 6) – a dilution effect. Ca and Mg at Grayson-Gunnar are also lower during similar periods; however, the amplitude of change is markedly less.

Results of nutrient chemistry and isotopes, including available forms of carbon, for discrete samples for the period March 21, 2015–September 5, 2015, are presented for Grayson-Gunnar in Fig. 7. PIC values contribute <0.3 mmol/L to the total carbon in the spring water; samples were not timed with pulses of suspended sediment. DIC concentrations range from 2.7 to 3.7 mmol/L, are generally greater

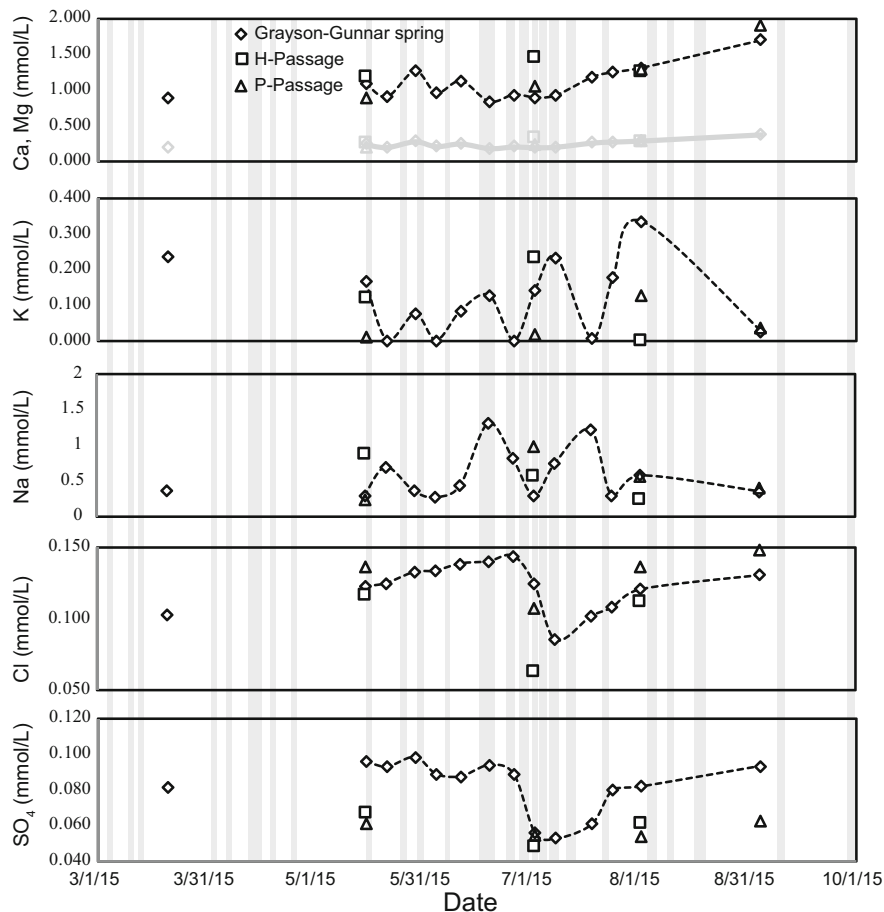


Fig. 6 Graphs of ion chemistry of discrete samples from Grayson-Gunnar karst basin spring through fall of 2015. Measurements performed using ion chromatography. Values of Mg estimated using a 44% contribution of dolomite and shown in light gray. Solid light-gray bars are periods of significant precipitation

later in the summer, and are higher than those measured at Sandy Springs (0.95–2.6 mmol/L) and much greater than measured at Stream Cave (0.13–0.81 mmol/L). Like Ca and Mg, DIC concentrations do not drop appreciably during periods of heavy rainfall. In contrast, DOC concentrations at Grayson-Gunnar, with average concentrations of 0.06 mmol/L, have spikes upward of 0.18 mmol/L associated with storm pulses. Average DOC concentrations at Sandy Springs are slightly higher (0.08 mmol/L) with lower peak concentrations (0.14 mmol/L); average concentrations at Stream Cave are also higher (0.09 mmol/L) with peak concentrations that are also greater (0.21 mmol/L).

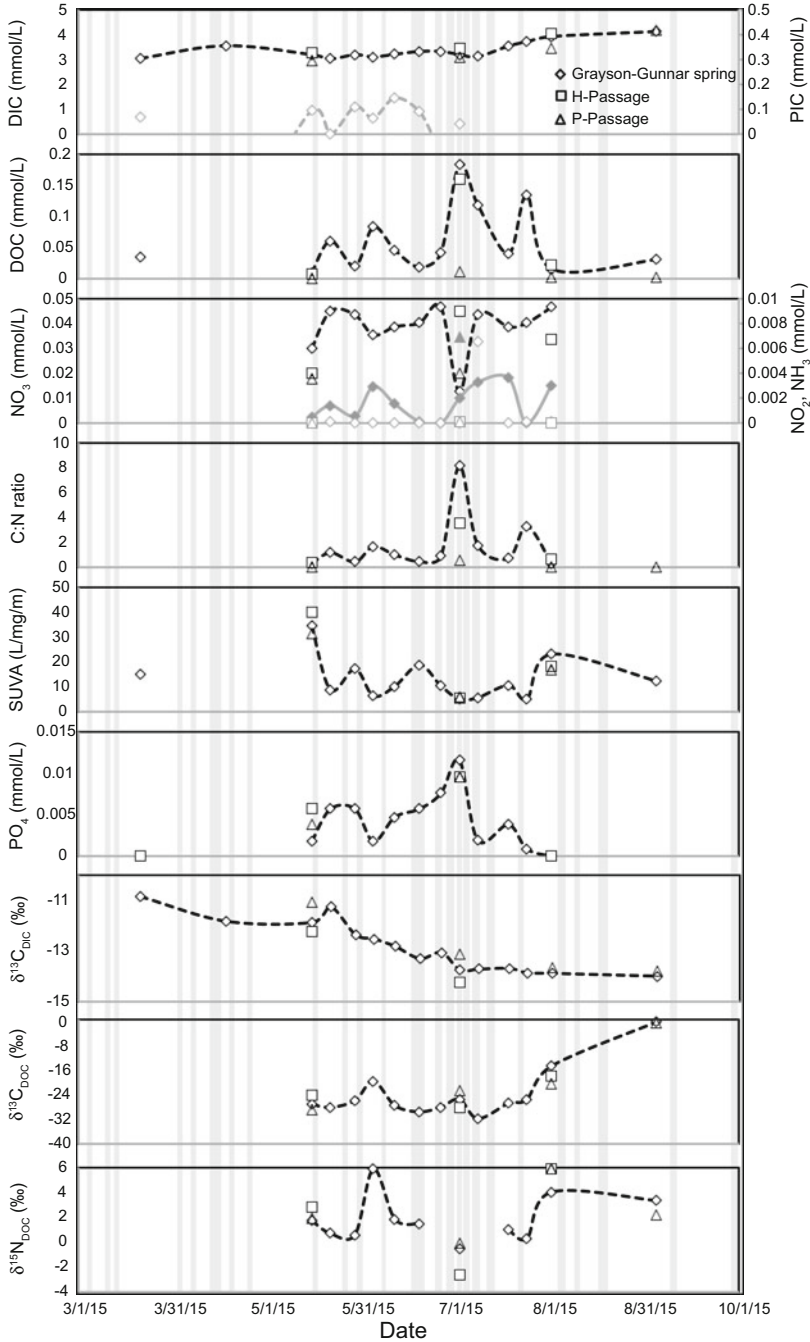


Fig. 7 Graphs of nutrient chemistry of discrete samples from Grayson-Gunnar karst basin spring through fall of 2015. DIC and PIC (light gray, top panel) measurements determined through field titrations. NH_3 (light gray, third panel) and NO_x (dark gray, third panel) and PO_4 measurements

Nitrate, nitrite, and unionized ammonia concentrations (Fig. 7) are below the drinking water limits of 0.16, 0.02, and 0.003 mmol/L, respectively, as established by the EPA and the Kentucky Administrative Regulations (401 KAR 10.031), with unionized ammonia (Y) computed by

$$Y = \frac{1.2[\text{NH}_3]}{1 + 10^{\text{pKa}-\text{pH}}} \quad (6)$$

where $\text{pKa} = 0.0902 + (2,730/(273 + T))$. The range of nitrate concentrations at Grayson-Gunnar (0.013–0.047 mmol/L) is lower than observed at Sandy Springs (0.02–0.08 mmol/L) but greater than concentrations at Stream Cave (0.0008–0.027 mmol/L). The average nitrate concentrations from all three exceed the average of 0.006 mmol/L for reference streams and rivers in the US Interior Plateaus EPA Ecoregion [61], although fall-winter measurements at Stream Cave fall below this reference stream value.

Nitrate concentrations at Grayson-Gunnar are inversely proportional to Q ; storm waters dilute this nutrient. The dilution combined with DOC spikes results in increased C:N molar ratios during storm events (Fig. 7), with ratios that range from 0.25 to 8.1. Nitrite and ammonia values at Grayson-Gunnar, on the other hand, spike during storm events because nitrified sources are conveyed during recharge; the concentrations range from below detection limit to 0.007 mmol/L for nitrite and up to 0.018 mmol/L for ammonia. The SUVA values range from 5 to 40 L/mg/m and are inversely proportional to DOC concentration and ammonia. Phosphate concentrations also spike during storm events as sediments to which they adhere are mobilized, and with concentrations that range from 0.002 to 0.008 mmol/L at GG, they significantly exceed the sample average of 0.0003 mmol/L from streams and rivers in the US Interior Plateaus EPA Ecoregion [61]. Nitrite, ammonia, SUVA, and phosphate data were not collected for Sandy Springs or Stream Cave.

The $\delta^{13}\text{C}_{\text{DIC}}$ at Grayson-Gunnar ranges from -14.0% to -10.9% and, with little exception, becomes progressively depleted in $^{13}\text{C}_{\text{DOC}}$ during the sampling period (Fig. 7). These values are more depleted than samples from Sandy Springs and Stream Cave that range from -12.4% to -7.3% and -6.3% to -9.4% , respectively. The $\delta^{13}\text{C}_{\text{DOC}}$ at GG ranges from -29.4% to 0.1% , with values that are enriched in $^{13}\text{C}_{\text{DOC}}$ at the conclusion the sampling period. At Sandy Springs and Stream Cave, the $\delta^{13}\text{C}_{\text{DOC}}$ has a narrow range of values that average $-27\% \pm 0.7\%$. $\delta^{15}\text{N}_{\text{DOC}}$ at Grayson-Gunnar ranges from -2.6% to 5.9% , with lower values during periods of significant precipitation and some similarities to the trends of both SUVA and $\delta^{13}\text{C}_{\text{DOC}}$. $\delta^{15}\text{N}_{\text{DOC}}$ values were not measured for either Sandy Springs or Stream Cave.

Fig. 7 (continued) performed using spectrophotometry. DOC measurements determined by persulfate digestion. SUVA determined at 254 nm. Values of $\delta^{13}\text{C}_{\text{DIC}}$ determined using CRDS. Values of $\delta^{13}\text{C}_{\text{DOC}}$ and $\delta^{15}\text{N}$ determined using IRMS. Solid light-gray bars are periods of significant precipitation

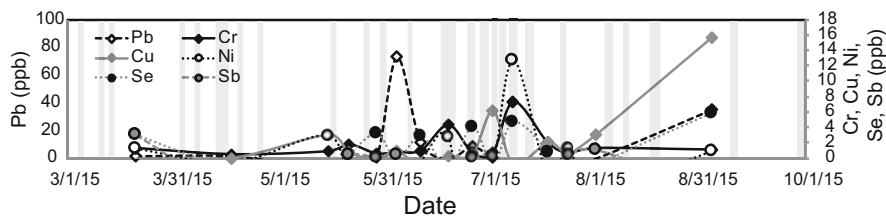


Fig. 8 Line graph showing select trace metal concentration of discrete samples from Grayson-Gunnar karst basin spring through fall of 2015. Measurements performed using chromatography. Solid light-gray bars are periods of significant precipitation

Concentrations of selected dissolved ($<0.45 \mu\text{m}$) trace metals (in ppb) for discrete samples for the period March 21, 2015–September 5, 2015, are presented for Grayson-Gunnar presented in Fig. 8. No trace metal data are available for either Sandy Springs or Stream Cave. Except for lead ($\text{Pb} = 16 \text{ ppb}$), the average concentration of trace metals ($\text{Cu} = 3.0 \text{ ppb}$, $\text{Se} = 2.7 \text{ ppb}$, $\text{Cr} = 1.7 \text{ ppb}$, $\text{Ni} = 3.6 \text{ ppb}$, $\text{Sb} = 0.7 \text{ ppb}$), as well as the concentrations from individual samples, are below the drinking water limits by the EPA and the Kentucky Administrative Regulations (401 KAR 10.031) ($\text{Pb} = 15 \text{ ppb}$, $\text{Cu} = 1,300 \text{ ppb}$, $\text{Se} = 20 \text{ ppb}$, $\text{Cr} = 100 \text{ ppb}$, $\text{Ni} = 610 \text{ ppb}$, $\text{Sb} = 5.6 \text{ ppb}$). Only two samples have lead concentrations that significantly exceed these limits, both from relatively dry periods and from samples that are more enriched in $^{13}\text{C}_{\text{DOC}}$ and $^{15}\text{N}_{\text{DOC}}$. Though variable, trace metal concentrations collectively are more elevated during periods of significant rainfall, likely because storm events mobilize sediments in which those metals are stored.

4.3 Continuous Monitoring

Figure 9 comprises the data at Grayson-Gunnar retrieved from the Aqua Troll 200 sonde (WL, T and SpC), average measured daily precipitation, and the computed PET. Over the estimated 496 ha of the Grayson-Gunnar karst basin, using the data during the period May 2017–September 2016, $1,890 \text{ m}^3$ of calculated recharge contributed to $1,990 \text{ m}^3$ of modeled discharge emerging from the Grayson-Gunnar spring, a water budget difference of 5.5%. This compares to a water budget difference of 8.8% using the same methods for the data from Sandy Springs. The average discharge at Sandy Springs is 26 L/s, which emerges from a karst basin estimated at 1,906 ha and is 2.2 times as large as the 12 L/s average for Grayson-Gunnar. The $Q_{\text{max}}/Q_{\text{mean}}$ ratios for both Grayson-Gunnar (5.7) and Sandy Springs (85) are reflects flashy behavior, common in conduit-dominated telogenetic karst [10].

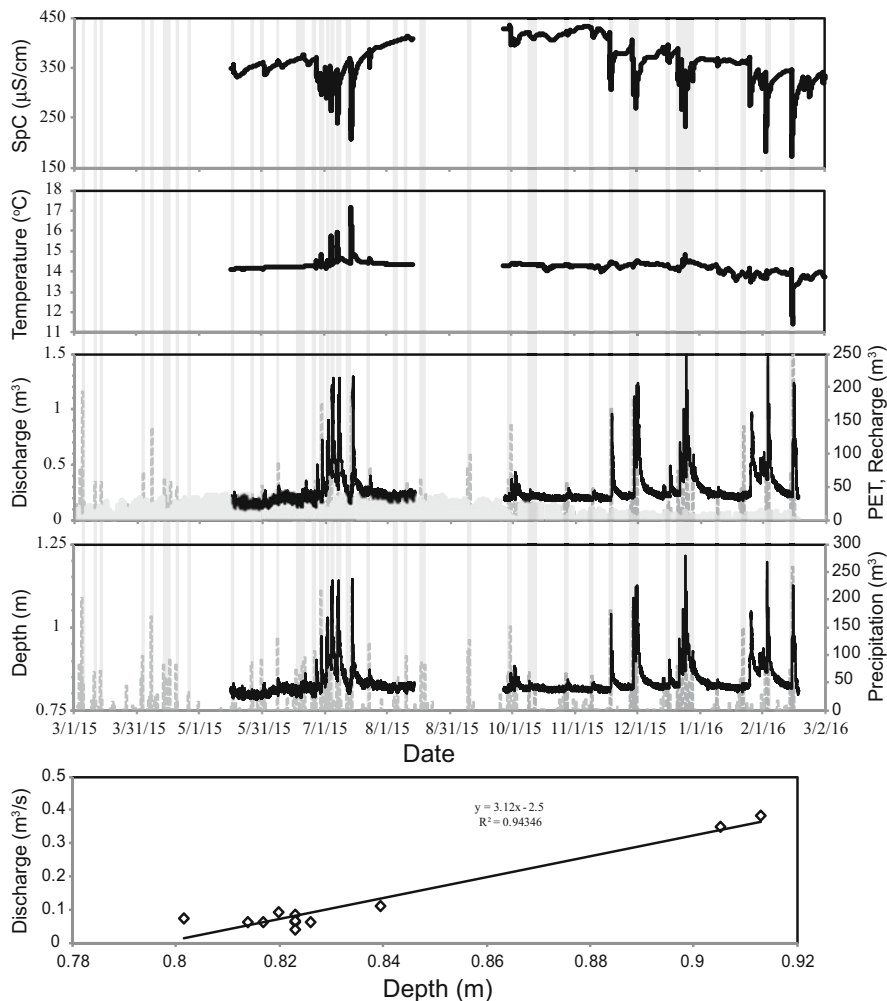


Fig. 9 Time series graphs of data from the Aqua Troll datasonde deployed at the Grayson-Gunnar spring May 2015 through February 2016. Rating curve between field measurements of discharge and water level in bottom panel. PET computed using the Priestly-Taylor method is shown as short light-gray bars in third panel. Precipitation shown as vertical dark-gray bars in middle panels. Solid light-gray bars are periods of significant precipitation

The recession limb of the hydrographs at Grayson-Gunnar generally occurs over 5 days with most declines in discharge occurring in the first day. In a summertime pattern (Fig. 10), pulses of recharge cause hydrographs with broad peaks and sharp, but brief, temperature spikes up to 17°C that include a shoulder on the receding limb. These time series temperature data also include a protracted peak of about 0.5°C above background conditions that occurs about 28 h after the initial recharge spike. Wintertime patterns do not reveal this same structure in the temperature data.

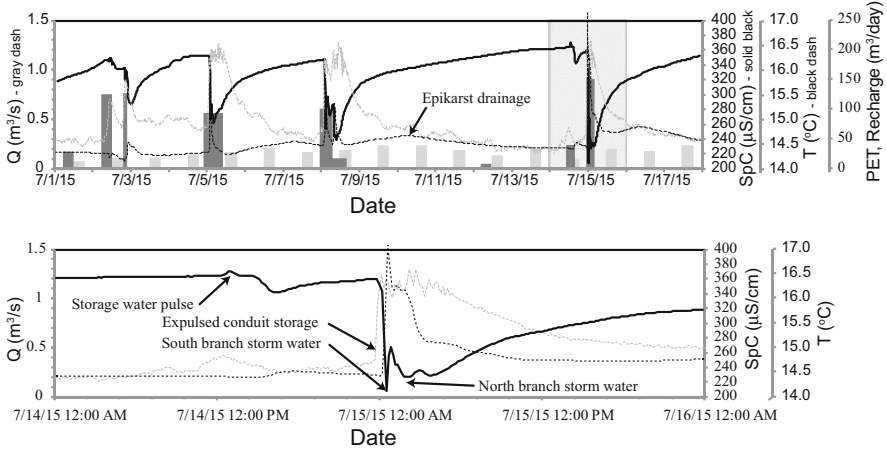


Fig. 10 Times series graphs of monitoring data from the Aqua Troll datasonde deployed at the Grayson-Gunnar spring (top panel) and computed discharge between July 1, 2015 and July 18, 2015 (bottom panel). PET computed using the Priestly-Taylor method is shown as short light-gray bars. Solid dark-gray bars are precipitation events. [Discharge – Q , specific conductance – SpC, temperature – T]. (Bottom panel) Zoom of Aqua Troll data between 7/14/2015 and 7/16/2015

SpC values are inversely proportional to discharge throughout the monitoring period as storm events move meteoric waters through the conduit system. Individual events at Grayson-Gunnar reveal a repeating pattern in the time series SpC data (Fig. 10) [55]: water of slightly higher conductance, stored in conduits, is forced from the aquifer followed by the arrival of lower conductivity meteoric waters. The arrival of this meteoric water comes in two pulses, the first is a sharp peak arriving with the first temperature spike, and the second is aligned with the shoulder of the temperature data.

Figure 11 includes the data at Grayson-Gunnar retrieved from the EXO2 sonde. Unfortunately, there is limited overlap in the summertime data between the two sondes to provide meaningful insight between Q , SpC, and the EXO2 parameters for this period. pH values range from 6.8 to 8.8 with an average value of 7.3; they trend toward lower, more stable values in the summer and higher, more variable values in the fall-winter with some alignment with changes in SpC. DO values range from 9.8 to 10.7 mg/L with an average value of 10.2 mg/L; values have similar trends in variation to pH. Values of fDOM (0–14.6 RFU, average of 2.5 RFU), phycocyanin (0–5.2 $\mu g/L$, average of 0.2 $\mu g/L$) and turbidity (0.12–2,200 FNU, average of 3.2 FNU) are strongly influenced by meteoric recharge which brings organic matter and sediment. The mean values of phycocyanin and turbidity are below the reference sample average of 3.85 $\mu g/L$ and 7.3 FNU, respectively, from streams and rivers in the US Interior Plateaus EPA Ecoregion [61]; both experience peak measurements that exceed these reference values.

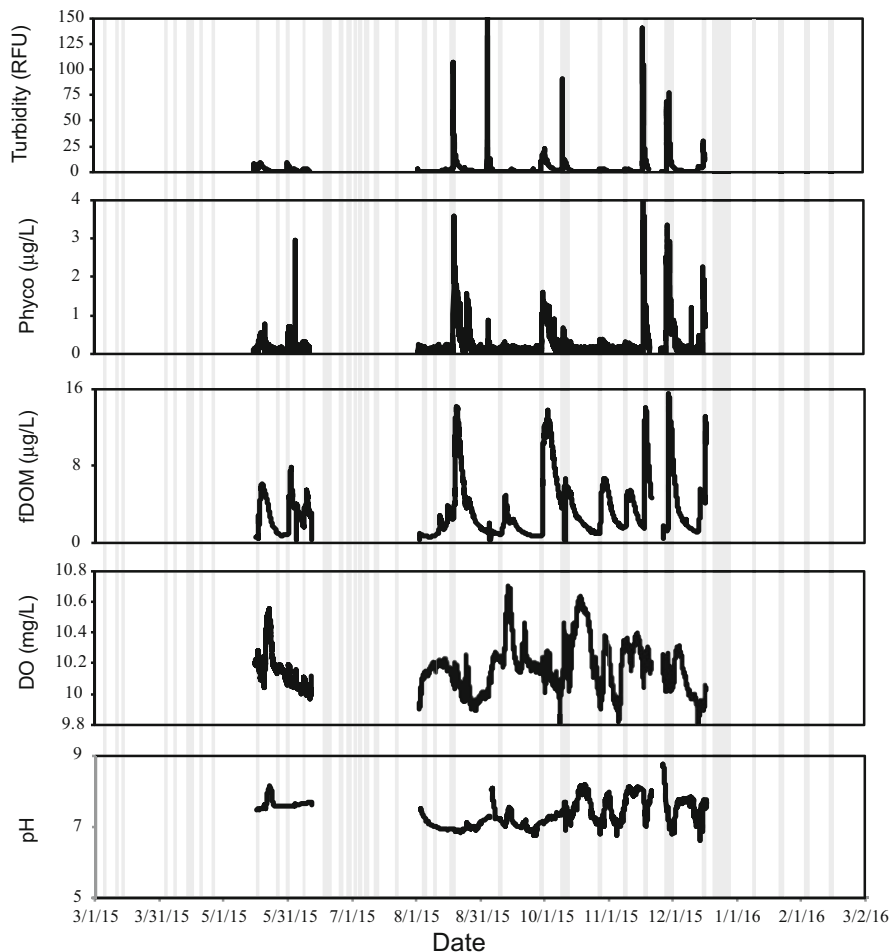


Fig. 11 Times series graphs of monitoring data from the EXO2 datasonde deployed at the Grayson-Gunnar spring May 2015 through December 2015. Solid light-gray bars are periods of significant precipitation

5 Discussion

5.1 Conduit Function

Both the Grayson-Gunnar and Redmond Creek karst basins have significant base flow overprinted with sizeable responses to all storm events that produce overland flow. At Grayson-Gunnar, the epikarst in Shearer Valley covers much of the basin increasing infiltration and storage, and when combined with the modulating effects of the series of rimstone dams along the underground flow path, the product is a spring response less flashy ($Q_{ratio} = 5.7$) than regional counterparts [10].

The contributions from epikarst storage in the Grayson-Gunnar karst basin convey waters with higher concentrations of the products of carbonate weathering (DIC, Ca, and Mg) leading to higher SpC and pH than at Sandy Springs. The concentrations of these ions are less variable than at Redmond Creek. At Sandy Springs, larger base flow is sourced to the alluvium that fills the sinkhole, providing significant storage and greater bedrock interaction; however, the surrounding plateau encompassing most of the basin contributes significant overland flow on steep hillslopes with limited infiltration. The result is a flashier response ($Q_{\text{ratio}} = 85$) and greater variability in DIC, Ca, and Mg [48].

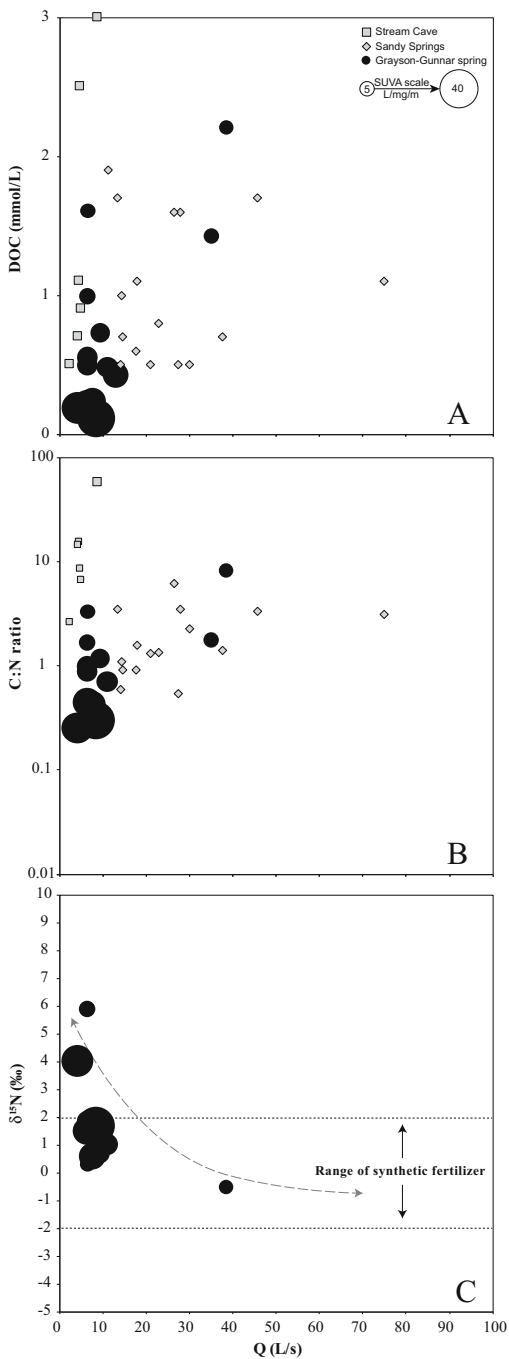
The two sub-basins within the Grayson-Gunnar karst basin have different lag times and thus produce separate excursions in the continuous monitoring data (Fig. 10). An initial pulse of storage water causes an initial spike in SpC as Q increases. Both sub-basins contribute flow at slightly different times: Q reaches maximum values almost instantaneously and, depending upon the amount and duration of precipitation, has two peaks or retains peak conditions for several hours before trailing off. Meteoric recharge from the smaller H-Passage sub-basin arrives within an hour having values of SpC and T that are largely unmixed with storage waters. The arrival of recharge from the larger P-Passage sub-basin occurs after 2 h with changes to SpC and T that are dampened and spread over a longer time frame due to greater mixing, thus creating the shoulder in the T data. The highly dampened peak in T more than a day after the storm event is likely linked to delayed recharge through the epikarst.

5.2 Chemical Processes

At Grayson-Gunnar, the concentration of DOC is directly, but not strongly, proportional to Q , and the SUVA values are inversely proportional to the concentration of DOC (Fig. 12a). Spikes in fDOM and phycocyanin in the continuous monitoring data coincide with storm events (Fig. 11) and more clearly demonstrate this relationship. Similar relationships exist when considering the C:N ratios of the samples (Fig. 12b), which have a mean value (1.8) lower than values in Cravotta [36] for manure land use. Higher discharge conditions, the product of storm events, convey additional organic matter that is more degraded from surface runoff. Those less degraded samples have a greater C:N ratio because the organic matter originates from surround forests.

At Spring Cave, the input to the Redmond Creek karst basin, DOC values have a wider variation and are more clearly proportional to Q ; the C:N ratios are significantly higher (average = 17.5). At Sandy Springs, the output to the Redmond Creek karst basin, DOC and C:N values have a narrower range with a mean C:N ratio (2.1) higher than the Grayson-Gunnar karst basin. The relationship at Sandy Springs between DOC and Q is visible but less clear; however, values fall below expectations at Grayson-Gunnar at the same value of DOC. The Grayson-Gunnar karst basin, with active flow paths mapped in detail through much of the basin, lies

Fig. 12 Scatter plots of (a) DOC, (b) C:N ratio, and (c) $\delta^{15}\text{N}$ data compared with discharge on x-axis. Values of $\delta^{15}\text{N}$ calibrated to atmospheric reference. Data from Grayson-Gunnar are shown with size proportional to values of SUVA



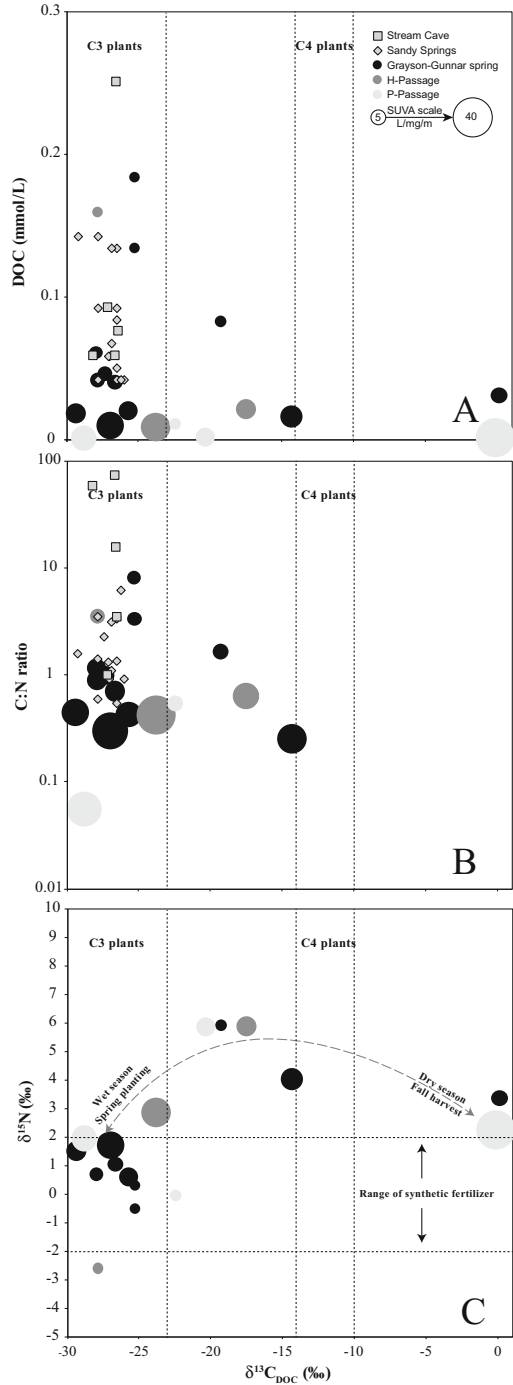
somewhere between the clear surface water signal at Stream Cave and the more modulated response at Sandy Springs that results from increased mixing and organic processing in the alluvium that characterizes part of that larger flow system.

In the Redmond Creek karst basin, Florea [28] reported $\delta^{13}\text{C}_{\text{DOC}}$ values at both Sandy Springs and Stream Cave within a quite narrow range and clearly within the expectations of C3-type vegetation (Fig. 13a), a product of the hardwood forests overlying most of the contributing watershed. In the Grayson-Gunnar karst basin, with more dominant agriculture and higher population density, the $\delta^{13}\text{C}_{\text{DOC}}$ values from all three sampling sites have a much broader range with some values that are clearly strongly influenced by C4-type vegetation and a few samples with values anonymously enriched in ^{13}C (Fig. 13a, c). Within the Grayson-Gunnar data, samples with higher DOC concentrations are more consistently in the range of C3-type vegetation and lower SUVA values. Samples with lower DOC concentrations and higher SUVA values are those with a broader $\delta^{13}\text{C}_{\text{DOC}}$ range. One interpretation is that the high-flow events correlate with times of surface runoff into sinking streams along the basin margin that bring organic matter from forest litter. The nitrogen data and nitrogen isotopes of the DOC tell a complementary story. There is a general relationship between lower ratios of $\delta^{15}\text{N}_{\text{DOC}}$, lower values of SUVA, and greater Q . The samples with lower $\delta^{15}\text{N}_{\text{DOC}}$ are mostly within the range expected from synthetic fertilizers [30] and align with lower C:N ratios, also seen in fertilizer land use from Cravotta [36]. This may reflect runoff of synthetic fertilizers in addition to the forest litter during storm events (Figs. 12a, c and 13c).

Base flow conditions convey infiltration water through the epikarst reservoir underlying the agricultural and residential areas of the sinkhole plain of Shearer Valley in the Grayson-Gunnar karst basin. Isotopic ratios during the driest conditions are enriched in ^{15}N above the range expected from synthetic fertilizers [30] (Fig. 12c). These samples were collected later in the discrete sampling program and have low DOC concentrations (Fig. 12a) and $\delta^{13}\text{C}_{\text{DOC}}$ values that correspond with C4-type vegetation (Fig. 13c). They may represent organic matter infiltrating the epikarst and carrying products of mature corn or corn-based animal feed or aromatic manure/septic waste from higher trophic levels (animals higher in the food chain) and a C4-based diet. The results are well within the published ranges for cow or poultry manure [36] but are more depleted in ^{15}N and more enriched in ^{13}C than spring waters from manure land use in that same study. The samples with anomalously high $\delta^{13}\text{C}_{\text{DOC}}$ values from the end of the sample period cannot be explained simply by contributions of waste from a C4-based diet.

At both the Sandy Springs and Grayson-Gunnar, average total nitrogen levels exceed 0.03 mmol/L as also found by the EPA in more than 58% of wells in groundwater agricultural watersheds [62]; samples from Stream Cave are considerably lower, centered upon the 0.16 mmol/L background concentration cited by Nolan and Hitt [63]. The source of the nitrogen, however, differs between the three sampling locations. At Grayson-Gunnar, both synthetic fertilizers and manure or septic waste have some influence (Fig. 13c) with proportions related to flow condition (Fig. 12c). The form of this nitrogen is also related to flow condition; nitrite and ammonia concentrations increase during periods of surface runoff (Fig. 7).

Fig. 13 Scatter plots of (a) DOC, (b) C:N ratio, and (c) $\delta^{15}\text{N}$ data compared with $\delta^{13}\text{C}_{\text{DOC}}$ on x -axis (VPBD standard). Values of $\delta^{15}\text{N}$ calibrated to atmospheric reference. Data from Grayson-Gunnar are shown with size proportional to values of SUVA



Nitrogen speciation or isotope data were not collected for Redmond Creek. Interestingly, average chloride and sulfate concentrations are also greater at Sandy Springs than for Grayson-Gunnar, both are significantly greater than for Stream Cave. Comparing chloride to total nitrogen helps to discriminate source (Fig. 14a). Samples from Stream Cave are tightly aligned and linearly proportional; they represent contributions from atmospheric deposition and forest litter (Fig. 14b). Samples from Sandy Springs have concentrations that are considerably more variable with two clusters: (1) a set that overlaps in range with the samples from Grayson-Gunnar and (2) a set with an enrichment of total nitrogen with increasing chlorides. This second set is the likely product of petroleum-related brines entrained in the flow system with well-documented effects on the geochemistry at Redmond Creek [48]. At Grayson-Gunnar, concentrations of chloride are less likely the result of brine and are more likely contributed from septic waste, animal waste, and road salts, evidenced by greater concentrations of potassium and sodium. These anthropogenic inputs also include phosphate (Fig. 7) and trace metals (Fig. 8), associated with turbidity produced during the storm events (Fig. 11) – either desorbed from sediment during changes in pH or bound to colloids ($<0.45 \mu\text{m}$).

6 Synthesis

The question this research originally set to resolve was whether the presence of the CAFO in the Grayson-Gunnar karst basin of south-central Kentucky, USA, constructed between 1997 and 2003, has led to specific changes in water quality. Additional inputs from residential septic waste, other livestock, and row-crop agriculture cloud that answer. However, compared to the nearby Redmond Creek karst basin with no CAFO and a land use principally composed of mixed hardwood, water quality differs in measurable ways. Those differences can be categorized into those that result from physical characteristics and those that are outcomes of land use.

Physical Characteristics The Redmond Creek karst basin receives considerable allogenic recharge from siliciclastics. Groundwater flow moves through the siliciclastic diamicton comprising the sinkhole alluvium and along the way entrains basin brines from shallow petroleum reservoirs in this downdip location on the margin of the Cumberland Plateau [48]. Resulting flow at Sandy Springs emerges slightly below saturation with respect to calcite ($-0.9 < SI < 0$) during elevated Q and above calcite saturation and ($0 < SI < 0.3$) during base flow as computed using the Debye Hückle relationship for the carbonate equilibrium reaction (Eq. 3). Storm events short circuit the groundwater flow system and produce sizable overland flow in the sinkhole and a flashy spring response [14, 16].

Flow emerging from the Grayson-Gunnar karst basin is also below saturation with respect to calcite ($-0.9 < SI < 0$) during elevated Q and above calcite saturation ($SI > 0.5$) during base flow when solutes from carbonate dissolution are significantly higher than seen at Sandy Springs. These solute concentrations are

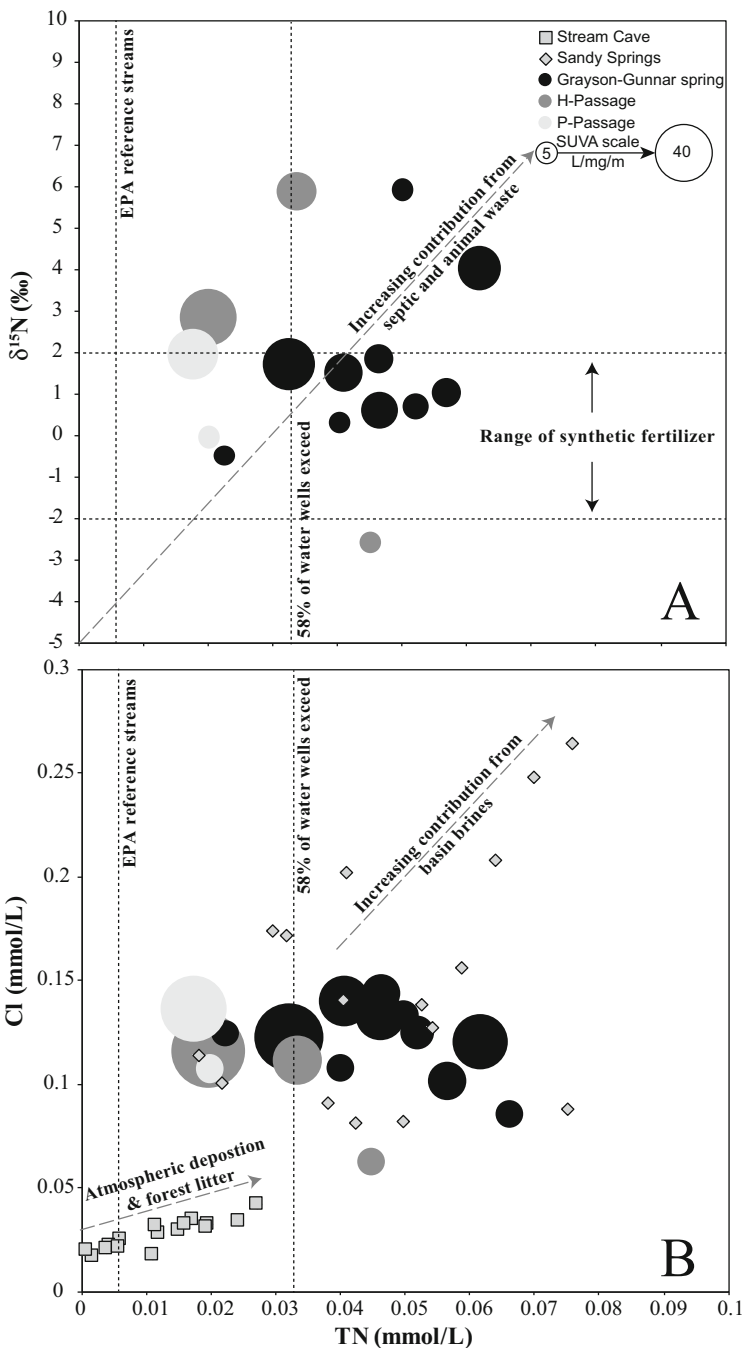


Fig. 14 Scatter plots of (a) $\delta^{15}\text{N}$ and (b) Cl data compared with total nitrogen on x-axis. Values of $\delta^{15}\text{N}$ calibrated to atmospheric reference. Data from Grayson-Gunnar are shown with size proportional to values of SUVA

greater, despite the smaller basin size, because substantial recharge is autogenic through the epikarst underlying the sinkhole plain that covers much of this basin situated updip of the Cumberland Escarpment. The reduced role of allogenic runoff from siliciclastics translates to a spring response less flashy than plateau-margin counterparts, also moderated by the damming effects of rimstone along the underground flow path. The two contributing sub-basins are discernable in continuous monitoring data of SpC and T as separate excursions; the smaller sub-basin responds more rapidly to a given storm event. Contributions through the epikarst to recharge are delayed by more than a day after onset of precipitation.

Land Use The rimstone that dams the underground flow path in Grayson-Gunnar appears to be dissolving and is covered with a thin film of clay; observations show no evidence of newly precipitated calcite and what is present has degraded. Has there been a change to the character of water? Perhaps in the recent past, Grayson-Gunnar spent more time in base flow conditions when storm events translated into less overland flow on a more forested landscape. Certainly the effects of agriculture are clearly observable in the chemical character of groundwater. Unlike Redmond Creek, where the isotopes of organic carbon are clearly and consistently within the range expected from a mixed hardwood forest with C:N ratios in headwater streams in the range expected from unaltered watersheds, values from Grayson-Gunnar have a wider range that are influenced by corn and animal waste from corn-based feed, particularly during base flow conditions. Nitrogen isotopes, SUVA, and C:N ratios of the organic carbon at Grayson-Gunnar illustrate the impact of synthetic fertilizers and recalcitrant carbon washed in during runoff and the leaching of more labile sources of carbon from higher trophic levels during base flow.

Headwater streams at Redmond Creek have nitrogen levels that hover near levels of reference streams measured by the EPA. The concentrations are significantly higher at both aquifer outputs, evidence of some human or agricultural impact; however, all measurements are below established drinking water limits. The source of nitrogen is different between the two karst basins: at Sandy Springs, excess nitrogen associates with basin brines from petroleum reservoirs; at Grayson-Gunnar, the excess nitrogen clearly associates with anthropogenic inputs. Phosphate levels at Grayson-Gunnar also exceed EPA reference streams with highest concentrations aligned with storm events that transmit high turbidity, organic carbon, and phyco-cyanin. These results suggest that these same storm events mobilize denitrified sources of nitrogen from animal waste and trace metals (such as copper, chromium, and selenium) that have an association with animal supplements.

Acknowledgments This project was funded, in part, by a Ralph Stone Fellowship from the National Speleological Society and grants from the Cave Research Foundation and the Geological Society of America. The author is grateful for the contributions to field sampling and analysis by Gilles Tagne, laboratory operations by Eric Lange, and assistance by other caver-colleagues. Immense gratitude to landowners Gary and Synda Heikkinen for access to their property and permission to sample and install equipment. Colleagues at the Indiana Geological and Water Survey and anonymous reviewers improved this manuscript.

References

1. White WB (1988) *Geomorphology and hydrology of karst terrains*. Oxford University Press, New York, 464 pp
2. Ford DC, Williams P (2007) *Karst hydrogeology and geomorphology*. Wiley, Hoboken, 562 pp
3. EPA (2002) State compendium – region 4. Programs and regulatory activities related to animal feeding operations, 64 pp. <https://www3.epa.gov/npdes/pubs/region4.pdf>. Accessed 14 Sept 2017
4. KDOW (August 2000) Animal Feeding Operations (AFO) & Concentrated Animal Feeding Operations (CAFO). Kentucky Division of Water. <http://water.nr.state.ky.us/dow/cafo.htm>. Accessed 5 Oct 2017
5. EPA (2004) NPDES profile: Kentucky. https://www3.epa.gov/npdes/pubs/kentucky_final_profile.pdf. Accessed 14 Sept 2017
6. EPA (2013) Literature review of contaminants in livestock and poultry manure and implications for water quality. U.S. Environmental Protection Agency, Office of Water, EPA 820-R-13-002, 125 pp
7. Burns RT, Xin H, Gates RS, Li H, Overhults DG, Moody L, Earnest J (2007) Ammonia emissions from broiler houses in the southern United States. In: Proceedings of the international symposium on air quality and waste management for agriculture, Broomfield, CO, 16–19 Sept. 2007. ASABE, St. Joseph
8. Brahana JV, Nix J, Bitting C, Bitting C, Quick R, Murdoch J, Roland V, Wets A, Robertson S, Scardale G, North V (2014) CAFOs on karst—meaningful data collection to adequately define environmental risk, with a specific application from the Southern Ozarks of Northern Arkansas. U.S. Geological Survey Scientific Investigations Report 2014–5035, pp 97–102
9. Kosić K, Bitting CL, Van Brahana J, Bitting CJ (2015) Proposals for integrating karst aquifer evaluation methodologies into national environmental legislations. *Sustain Water Resour Manag* 1(4):363–374. <https://doi.org/10.1007/s40899-015-0032-5>
10. Florea LJ, Vacher HL (2006) Springflow hydrographs: eogenetic versus telogenetic karst. *Ground Water* 44(3):352–361
11. Dreiss SJ (1982) Linear kernels for karst aquifers. *Water Resour Res* 18(4):865–876
12. Hobbs SL, Smart PL (1986) Characterization of carbonate aquifers; a conceptual base. In: Proceedings of the environmental problems in karst terranes and their solutions conference, Bowling Green, KY. National Water Well Association, Dublin, pp 1–14
13. Shuster ET, White WB (1971) Seasonal fluctuations in the chemistry of limestone springs: a possible means for characterizing carbonate aquifers. *J Hydrol* 14(2):93–128
14. Simpson LC, Florea LJ (2009) The Cumberland Plateau of Eastern Kentucky. In: Palmer AN, Palmer MV (eds) *Caves and karst of America*. National Speleological Society, Huntsville, pp 70–79
15. Atkinson TC (1977) Diffuse flow and conduit flow in limestone terrain in the Mendip Hills, Somerset (Great Britain). *J Hydrol* 35(1–2):93–110
16. Florea LJ (2013) Selective recharge and isotopic composition of shallow groundwater within temperate, epigenetic carbonate aquifers. *J Hydrol* 489:201–213. <https://doi.org/10.1016/j.jhydrol.2013.03.008>
17. Scanlon BR (1989) Physical controls on hydrochemical variability in the Inner Bluegrass Karst Region of Central Kentucky. *Ground Water* 27(5):639–646
18. Desmarais K, Rojstaczer S (2002) Inferring source waters from measurements of carbonate spring response to storms. *J Hydrol* 260(1–4):118–134
19. Ryan MT, Meiman J (1996) An examination of short-term variations in water quality at a karst spring in Kentucky. *Ground Water* 34(1):23–30
20. Kendall C, Caldwell EA (1998) Fundamentals of isotope geochemistry. In: Kendall C, McDonnell JJ (eds) *Isotope tracers in catchment hydrology*. Elsevier Science B.V., Amsterdam, pp 51–86
21. Schlesinger WH (1997) *Biogeochemistry: an analysis of global change*. Academic Press, San Diego, 443 pp

22. Ehleringer JR, Buchmann N, Flanagan LB (2000) Carbon isotope ratios in belowground carbon cycle processes. *Ecol Appl* 10(2):412–422
23. Weishaar JL, Aiken GR, Bergamaschi BA, Fram MS, Fujii R, Mopper K (2003) Evaluation of specific ultraviolet absorbance as an indicator of the chemical composition and reactivity of dissolved organic carbon. *Environ Sci Technol* 37:4702–4708
24. Clark I, Fritz P (1997) *Environmental isotopes in hydrogeology*. Lewis Publishers, New York, 352 pp
25. Deines P, Langmuir D, Harmon RS (1974) Stable carbon isotope ratios and the existence of a gas phase in the evolution of carbonate ground waters. *Geochim Cosmochim Acta* 38:1147–1164
26. Marlier JF, O’Leary MH (1984) Carbon kinetic isotope effects on the hydration of carbon dioxide and the dehydration of bicarbonate ion. *J Am Chem Soc* 106:5054–5057
27. Berner RA, Lasaga AC, Garrels RM (1983) The carbonate–silicate cycle and its effect on atmospheric carbon dioxide over the past 100 million years. *Am J Sci* 284:641–683
28. Florea LJ (2013) Isotopes of carbon in a karst aquifer of the Cumberland Plateau of Kentucky. *Acta Carsol* 42(2–3):277–289
29. Vitousek PM, Aber JD, Howarth RH, Likens GE, Matson PA, Schindler DW, Schlesinger WH, Tilman DG (1997) Human alteration of the global nitrogen cycle: source and consequences. *Ecol Appl* 7:737–750
30. Bateman AS, Kelly SD (2007) Fertilizer nitrogen isotope signatures. *Isot Environ Health Stud* 43(3):237–247
31. Craine JM, Brookshire ENJ, Cramer MD et al (2015) Ecological interpretations of nitrogen isotope ratios of terrestrial plants and soils. *Plant Soil* 396(1–2):1–26. <https://doi.org/10.1007/s11104-015-2542-1>
32. Craine JM, Towne EG, Ocheltree TW, Nippert JB (2012) Community traitscape of foliar nitrogen isotopes reveals N availability patterns in a tallgrass prairie. *Plant Soil* 356:395–403
33. Holá M, Ježek M, Kušta T, Košatová M (2015) Trophic discrimination factors of stable carbon and nitrogen isotopes in hair of corn fed wild boar. *PLoS One* 10(4):e0125042. <https://doi.org/10.1371/journal.pone.0125042>
34. Inácio CT, Urquiaga S, Chalk PM (2013) Nitrogen and carbon isotope composition of organic fertilizers. In: XXXIV Congresso Brasileiro de Ciencia do Solo. Costao do Santinho Resort, Florianopolis
35. Brady NC, Weil RR (2002) *The nature and properties of soils*, 13th edn. Prentice Hall, Upper Saddle River
36. Cravotta CA (1997) Use of stable isotopes of carbon, nitrogen, and sulfur to identify sources of nitrogen in surface waters in the Lower Susquehanna River Basin, Pennsylvania. U.S. Geological Survey Water-Supply Paper 2497, 99 pp
37. EPA (2013) Level III ecoregions of the continental United States: Corvallis, Oregon, U.S. EPA – National Health and Environmental Effects Research Laboratory, map scale 1:7,500,000. http://www.epa.gov/wed/pages/ecoregions/level_iii_iv.htm. Accessed 5 Oct 2017
38. Palmer AN (1987) Cave levels and their interpretation. *NSS Bull* 49:50–66
39. Granger DE, Fabel D, Palmer AN (2001) Plio-Pleistocene incision of the Green River, KY from radioactive decay of cosmogenic ²⁶Al and ¹⁰Be in Mammoth Cave sediments. *GSA Bull* 113(7):825–836
40. Chester EW, Noel SM, Baskin JM, Baskin CC, McReynolds ML (1995) A phytosociological analysis of an old-growth upland wet woods on the Pennyroyal Plain, southcentral Kentucky, USA. *Nat Areas J* 15:297–307
41. Drummond M (2016) Interior Plateau. <https://landcover.trends.usgs.gov/east/eco71Report.html>. Accessed 14 Sept 2017
42. Turner JA, Oswalt CM, Chamberlain JL, Conner RC, Johnson TG, Oswalt SN, Randolph KC (2008) *Kentucky’s Forests, 2004*. USFS Southern Research Station. Resource Bulletin SRS-129
43. USFS (2006) Property taxation, forest fragmentation and development in Kentucky’s Green River and Lower Cumberland River watersheds. Report as of FY2006 for 2006KY67B

44. Ettensohn FR, Rice CR, Dever GR Jr, Chesnut DR (1984) Slade and paragon formations; new stratigraphic nomenclature for Mississippian rocks along the Cumberland Escarpment in Kentucky. *U.S. Geological Survey Bulletin* 1605-B, 37 pp
45. Sasowsky ID, White WB, Schmidt VA (1995) Determination of stream-incision rate in the Appalachian plateaus by using cave sediment magnetostratigraphy. *Geology* 23:415–418
46. Anthony DM, Granger DE (2004) A late tertiary origin for multilevel caves along the western escarpment of the Cumberland plateau, Tennessee and Kentucky, established by cosmogenic ^{26}Al and ^{10}Be . *J Cave Karst Stud* 66(2):46–55
47. Anthony DM, Granger DE (2007) A new chronology for the age of Appalachian erosional surfaces determined by cosmogenic nuclides in cave sediments. *Earth Surf Process Landf* 32:874–887
48. Florea LJ (2015) Carbon flux and landscape evolution in epigenetic karst aquifers modeled from geochemical mass balance. *Earth Surf Process Landf* 40(8):1072–1087. <https://doi.org/10.1002/esp.3709>
49. Crawford NC (1984) Karst landform development along the Cumberland Plateau Escarpment of Tennessee. In: LeFleur RG (ed) *Groundwater as a geomorphic agent*. Allen and Unwin, Inc., Boston, pp 294–338
50. Palmer AN (1991) Origin and morphology of limestone caves. *Geol Soc Am Bull* 103:1–21
51. Sasowsky ID, White WB (1994) The role of stress release fracturing in the development of cavernous porosity in carbonate aquifers. *Water Resour Res* 30(12):3523–3530
52. Florea LJ, Blair RJ (2014) 2013–2014 Dye trace activities in the Cumberland Plateau of Southeast Kentucky. In: 2014 National Speleological Society convention program guide
53. Florea LJ, Stinson CL, Lawhon N, Walden WD, Zhu J, Webb S (2011) Electrical resistivity tomography surveys in an Alluviated Karst Valley in Southeast Kentucky. In: 2011 National Speleological Society convention program guide
54. Florea LJ (2013) Investigations into the potential for hypogene speleogenesis in the Cumberland plateau of Southeast Kentucky, U.S.A. In: *Proceedings of the 16th international congress of speleology, Brno, Czech Republic, July 2013*, pp 356–361
55. Florea LJ (2017) Sulfur-based speleogenetic processes in the Cumberland Plateau, USA. In: Klimchouk AB, Palmer AN, De Waele J, Auler AS, Audra P (eds) *Hypogene karst and caves of the world*. Springer, Berlin, pp 683–690
56. Paylor RL (2016) Particulate inorganic carbon flux and sediment transport dynamics in karst: significance to landscape evolution and the carbon cycle. Dissertation, Louisiana State University, Baton Rouge, 148 pp
57. Jones JK, Florea LJ, Rust DL, Miller R (2015) Isotope stratigraphy of the Viséan carbonates in the St. Louis and Ste. Genevieve members of the slade formation in southeast Kentucky. *Geol Soc Am Abstr Programs* 47(2):28
58. Rantz SE (1982) Measurement and computation of streamflow, volume 1, measurement of stage and discharge. United States Geological Survey Water Supply Paper 2175, 284 pp
59. Rounds SA (2012) Alkalinity and acid neutralizing capacity. In: TWRI Book 9 Chapter A6. United States Geological Survey, Reston
60. Priestley CHB, Taylor RJ (1972) On the assessment of surface heat flux and evaporation using large-scale parameters. *Mon Weather Rev* 100:81–82
61. EPA (2000) Ambient water quality criteria recommendation information supporting the development of state and tribal nutrient criteria for rivers and streams in nutrient ecoregion IX: Southeastern Temperate Forested Plains and Hills including all or parts of the States of Maryland, Pennsylvania, Virginia, North Carolina, South Carolina, Georgia, Florida, Alabama, Mississippi, Tennessee, Kentucky, Indiana, Illinois, Iowa, Missouri, Kansas, Oklahoma, Arkansas, Louisiana, Texas and the authorized Tribes within the Ecoregion. U.S. Environmental Protection Agency, Office of Water, EPA 822-B-00-019
62. EPA (n.d.) Report on the environment. Nitrate and pesticides in shallow ground water in agricultural watersheds. <https://cfpub.epa.gov/roe/indicator.cfm?i=36>. Accessed 5 Oct 2017
63. Nolan BT, Hitt KJ (2002) Nutrients in shallow ground waters beneath relatively undeveloped areas in the conterminous United States. U.S. Geological Survey water resources investigation report 02-4289, 21 pp